Low-Lying Electronic States of $M_3O_9^-$ and $M_3O_9^{2-}$ (M = Mo, W)

Shenggang Li and David A. Dixon*

Department of Chemistry, The University of Alabama, Shelby Hall, Box 870336, Tuscaloosa, Alabama 35487-0336

Received: May 30, 2007; In Final Form: July 30, 2007

Multiple low-lying electronic states of $M_3O_9^-$ and $M_3O_9^{2-}$ (M = Mo, W) arise from the occupation of the near-degenerate low-lying virtual orbitals in the neutral clusters. We used density functional theory (DFT) and coupled cluster theory (CCSD(T)) with correlation consistent basis sets to study the structures and energetics of the electronic states of these anions. The adiabatic and vertical electron detachment energies (ADEs and VDEs) of the anionic clusters were calculated with 27 exchange-correlation functionals including one local spin density approximation functional, 13 generalized gradient approximation (GGA) functionals, and 13 hybrid GGA functionals, as well as the CCSD(T) method. For $Mo_3O_9^-$, CCSD(T) and nearly all of the DFT exchange-correlation functionals studied predict the $^2A_1$ state arising from the Jahn−Teller distortion due to singly occupying the degenerate e′ orbital to be lower in energy than the $^2A_1'$ state arising from singly occupying the nondegenerate a_1' orbital. For $W_3O_9^-$, the $^2A_1$ state was predicted to have essentially the same energy as the $^2A_1'$ state at the CCSD(T) level with core-valence correlation corrections included and to be higher in energy or essentially isoenergetic with most DFT methods. The calculated VDEs from the CCSD(T) method are in reasonable agreement with the experimental values for both electronic states if estimates for the corrections due to basis set incompleteness are included. For $M_3O_9^{2-}$, the singlet state arising from doubly occupying the nondegenerate a_1' orbital was predicted to be the most stable state for both M = Mo and W. However, whereas $Mo_3O_9^{2-}$ was predicted to be less stable than $Mo_3O_9^-$, $W_3O_9^{2-}$ was predicted to be more stable than $W_3O_9^-$.

Introduction

There is substantial interest in aromatic molecules, especially in metallic systems.[1] Anionic photoelectron spectroscopy (PES) experiments have recently been performed by Sun et al.[2] for $(WO_3)_n^-$ (n = 1−4) and by Huang et al.[3] for $M_3O_9^-$ (M = Mo, W). Adiabatic and vertical electron detachment energies (ADEs and VDEs) were measured. Huang et al.[3] predicted the $^2A_1'$ state in D_{3h} symmetry to be the ground state of $M_3O_9^-$ on the basis of density functional theory (DFT)[4,5] calculations with the B3LYP exchange-correlation functional[6−8] and extended basis sets with effective core potentials on the metals. The experimental spectrum for the transition from the ground state of $M_3O_9^-$ to that of M_3O_9 exhibits a broad profile, indicative of large geometry changes upon electron detachment. This was attributed to a strong metal−metal σ-bonding interaction in the ground state of $M_3O_9^-$, absent in that of M_3O_9. Huang et al.[3] concluded that d-d resonance (d-orbital aromaticity) was present in $M_3O_9^-$ and $M_3O_9^{2-}$ on the basis of calculated resonance energies, orbital compositions, and nucleus-independent chemical shifts.[9] However, in our recent DFT studies on the $(MO_3)_n$ (M = Cr, Mo, W; n = 1−6) clusters, we showed that the lowest unoccupied molecular orbital (LUMO) of M_3O_9 is of e' symmetry, and that the next LUMO is of a_1' symmetry.[10] The energy difference between these two virtual orbitals was predicted to be 8.7 kcal/mol for M = Mo and 0.7 kcal/mol for M = W at the B3LYP level with the aug-cc-pVDZ basis set for oxygen[11,12] and the Stuttgart small core relativistic effective core potential (ECP) basis set for Mo and W (ECP28MWB and ECP60MWB).[13] Occupation of the a_1' virtual orbital in M_3O_9 by the unpaired electron in $M_3O_9^-$ results in the $^2A_1'$ state in D_{3h} symmetry as found by Huang et al.[3], whereas occupation of the e' virtual orbital results in a Jahn−Teller distortion leading to a state with lower symmetry. As the orbitals are very close in energy, either state could be the ground electronic state of the anion. In fact, our time-dependent DFT (TD-DFT) calculations[14−16] at the B3LYP level with the above basis set on M_3O_9 revealed three closely lying excited electronic states, with excitation energies of 3.97, 3.99, and 3.99 eV for the singlets and 3.55, 3.55, and 3.58 eV for the triplets for M = Mo, and 4.29, 4.30, and 4.30 eV for the singlets and 4.01, 4.01, and 4.02 eV for the triplets for M = W, consistent with the simple orbital picture for the neutral cluster.[10]

In the current study, we have used both DFT and coupled cluster theory with single and double excitations and perturbative triple corrections (CCSD(T))[17−20] to calculate the structures and energetics of these electronic states and compared the calculated ADEs and VDEs with their experimental values. As part of our DFT calculations, we evaluated the performance of 27 exchange-correlation functionals.

Computational Methods

DFT calculations were carried out for the neutral clusters and their mono- and dianions. Geometries were optimized with the B3LYP exchange-correlation functional. Energies were calculated with a variety of exchange-correlation functionals at the B3LYP-optimized geometries. The exchange-correlation functionals studied include the local spin density approximation functional SVWN5;[21,22] the generalized gradient approximation (GGA) functionals BLYP,[6,8] BP86,[6,23] BPW91,[6,24] BB95,[6,25] PW91,[24,26] mPWPW91,[24,27] PBE,[28,29] OLYP,[8,30] TPSS,[31] VSXC,[32]

* Corresponding author. E-mail: dadixon@bama.ua.edu.

10.1021/jp074187t CCC: $37.00
Published on Web 10/11/2007

and the Handy family of functionals HCTH93, HCTH147, HCTH407;[33−35] and the hybrid GGA functionals B3LYP, B3P86, B3PW91,[7] B1B95,[25] B1LYP, mPW1PW91,[36] B98,[37] B971,[38] B972,[39] PBE1PBE,[28] O3LYP,[40] TPSSh,[31] and BMK.[41] All DFT calculations were carried out with the Gaussian 03 program package.[42]

Energies were also calculated at the CCSD(T) level.[17−20] All CCSD(T) calculations were done with the MOLPRO 2006.1[43] and NWChem 5.0[44,45] program packages. The open-shell calculations were done with the R/UCCSD(T) approach where a restricted open-shell Hartree−Fock (ROHF) calculation is initially performed and the spin constraint is then relaxed in the coupled cluster calculation.[46−48] We note that the calculated (*T*) contributions are slightly different in the MOLPRO and NWChem implementations for R/UCCSD(T).

The B3LYP geometry optimizations were done with the augmented correlation consistent double-ζ (aug-cc-pVDZ) basis set for O,[12] and the aug-cc-pVDZ-PP ECP basis sets for Mo and W.[49] These basis sets are collectively denoted as aD. In addition, we also optimized these geometries at the B3LYP level with the aug-cc-pVTZ basis set for O,[12] and the ECP28MWB basis set for Mo and the ECP60MWB basis set for W,[13] augmented with two f and one g functions as recommended by Martin and Sundermann.[50] These basis sets are collectively denoted as aT-ECP. The DFT energy calculations were carried out with the aug-cc-pVTZ basis set for O,[12] and the aug-cc-pVTZ-PP basis sets for Mo and W,[29] denoted as aT. CCSD(T) energy calculations were also done with the aD, aD-ECP, aT, and aT-ECP basis sets. Furthermore, core-valence correlation corrections were evaluated at the CCSD(T) level with the aug-cc-pwCVDZ basis set for O,[51,52] and aug-cc-pwCVDZ-PP basis sets for Mo and W.[49]

The calculations were done on the Opteron-based Cray XD1 and Itanium 2-based Altix supercomputers at the Alabama Supercomputer Center, on the Xeon-based Dell Linux cluster at the University of Alabama, on the local Opteron-based Parallel Quantum Solutions Linux cluster, and on the Itanium 2-based Linux cluster at the Molecular Science Computing Facility at the Pacific Northwest National Laboratory.

Results and Discussion

Geometries and Relative Energies. Optimized geometries at the B3LYP/aD and B3LYP/aT-ECP levels are given in Table 1 for the different electronic states of M_3O_9, $M_3O_9^-$, and $M_3O_9^{2-}$ (M = Mo, W). We used the Cartesian coordinate system and geometry parameters shown in Figure 1. Our results with the B3LYP/aT-ECP method are identical to those obtained by Huang et al.[3] with the same method for the $^1A_1'$ state of M_3O_9, the $^2A_1'$ state of $M_3O_9^-$, and the $^1A_1'$ state of $M_3O_9^{2-}$ as expected. Furthermore, the optimized geometries using the aD and aT-ECP basis sets are essentially identical, so we base our discussion on the aD results. The ground state of M_3O_9 was predicted to be the $^1A_1'$ state in D_{3h} symmetry as shown previously.[3,10] The LUMO is a doubly degenerate orbital with e' symmetry dominated by metal d orbitals in the *xy* plane as shown in Figure 2a. The next lowest unoccupied orbital (NLUMO) is of a_1' symmetry, which is also dominated by metal d orbitals in the *xy* plane as shown in Figure 2b. The primary difference between these two sets of orbitals is the localization of the metal orbitals for the e' orbitals due to the requirement for orthogonality. The a_1' orbital lies 11.6 and 3.8 kcal/mol higher in energy than the e' orbital at the B3LYP/aD level for M = Mo and W, respectively. Addition of an electron to M_3O_9 to form $M_3O_9^-$ can result in the occupation of either the a_1' orbital to form the $^2A_1'$ state in D_{3h} symmetry or the e' orbital to form a Jahn−Teller distorted state in lower symmetry. Two Jahn−Teller distorted states in C_{2v} symmetry, the $^2A_1$ and $^2B_2$ states, were predicted as expected.[53] Compared with the $^1A_1'$ state of M_3O_9, the $^2A_1'$ state of $M_3O_9^-$ has slightly longer M═O and M−O bond lengths (by ∼0.02 Å) and similar O═M═O bond angles, but much larger O−M−O bond angles (by ∼20°). For the $^2A_1$ and $^2B_2$ states, the M−O bond lengths differ by up to 0.2 Å and range above and below the value in the $^2A_1'$ state. The O═M═O and O−M−O bond angles differ from each other in these two states by up to 20°. One set of O−M−O bond angles in the $^2A_1$ and $^2B_2$ states is comparable to that in the neutral and the other is much smaller. Both bond angles in the $^2A_1$ and $^2B_2$ states are substantially smaller than the ones in the $^2A_1'$ state. The triangles formed by the three metal atoms in the $^2A_1$ and $^2B_2$ states deviate from an equilateral triangle, with the unique M−M−M angle in the $^2A_1$ state of ∼55° and that in the $^2B_2$ state of ∼63°. The $^2B_2$ state has one imaginary frequency, 356 and 308 cm^{-1} for M = Mo and W, respectively, although no lower energy conformation was found by further lowering the symmetry. This is consistent with previous work on other triangle-shaped systems dominated by a conical intersection at the equilateral triangle geometry.[54,55] As shown by Huang et al.,[3] the singly occupied molecular orbital (SOMO) of the $^2A_1'$ state in Figure 2c displays strong metal d orbital overlap. However, no such overlap was found for the SOMOs of the $^2A_1$ and $^2B_2$ states (Figure 2d,e). This is consistent with the above discussion for the LUMOs of M_3O_9. The electron spin densities are consistent with the orbital descriptions with the spin density for the $^2A_1'$ state shown in Figure 3a displaying a large electron density inside the six-member metal−oxygen ring, whereas the spin densities for the $^2A_1$ and $^2B_2$ states shown in Figures 3b and 3c exhibit no such character.

For $M_3O_9^{2-}$, three possible electron configurations, $(a_1')^2$, $(e')^2$, and $(e')^1(a_1')^1$, were considered. Only the $^1A_1'$ state arising from $(a_1')^2$ and the $^3A_2'$ state arising from $(e')^2$ are not subject to Jahn−Teller distortions. The Jahn−Teller distorted states are the $^1A_1$, $^3A_1$, and $^3B_2$ states, with two $^1A_1$ states arising by doubly occupying each of the two e' orbitals. Compared with the $^2A_1'$ state of $M_3O_9^-$, the $^1A_1'$ state of $M_3O_9^{2-}$ has slightly longer M═O bonds (by ∼0.02 Å), similar M−O bond lengths and O═M═O bond angles, and larger O−M−O angles (by ∼10°). The $^3A_2'$ state, on the other hand, has much smaller O−M−O angles (by ∼30°). The $^1A_1$, $^3A_1$, and $^3B_2$ states of $M_3O_9^{2-}$ have varying bond lengths and bond angles as in the case of $M_3O_9^-$. The $^3A_2'$ state has two imaginary frequencies, both of ∼150 cm^{-1} for M = Mo and ∼320 cm^{-1} for M = W. One of the $^1A_1$ states has an imaginary frequency, 85 and 75 cm^{-1} for M = Mo and W, respectively. The $^3B_2$ state of $W_3O_9^{2-}$ also has one imaginary frequency of 581 cm^{-1}.

Relative energies for the different electronic states of $M_3O_9^-$ and $M_3O_9^{2-}$ at the B3LYP and CCSD(T) levels are listed in Table 2. At the CCSD(T)/aT level, the ground state of $M_3O_9^-$ was predicted to be the $^2A_1$ state. The $^2A_1'$ state of $M_3O_9^-$ was calculated to be higher in energy than the $^2A_1$ state by 7.5 and 1.1 kcal/mol for M = Mo and W, respectively. With core-valence correlation corrections at the CCSD(T)/aug-cc-pwCVDZ/aug-cc-pwCVDZ-PP level, the $^2A_1'$ state of $Mo_3O_9^-$ is higher in energy than the $^2A_1$ state by 6.3 kcal/mol. For M = W, these two states have essentially the same energy. Thus, the effect of core-valence corrections is to lower the energy of the $^2A_1'$ states relative to the $^2A_1$ states by about 1.2 kcal/mol. The ground state of $M_3O_9^{2-}$ was predicted to be the $^1A_1'$ state with all of the other states for $M_3O_9^{2-}$ higher in energy than the $^1A_1'$ state

TABLE 1: Optimized Metal Oxygen Bond Lengths (Angstroms) and Bond Angles (Degrees) for the Different Electronic States of $M_3O_9^{n-}$ (M = Mo, W; $n = 0-2$) at the B3LYP Level with the aD and aT-ECP Basis Sets[a]

		M=O			M−O		O=M=O		O−M−O	
state	basis set	*a*	*b*	*c*	*d*	*e*	α	*β*	*γ*	*δ*
					Mo_3O_9					
$^1A_1'$	aD	1.689			1.902		107.7		103.5	
	aT-ECP	1.680			1.896		107.8		102.9	
					$Mo_3O_9^-$					
$^2A_1'$	aD	1.711			1.918		110.2		121.7	
	aT-ECP	1.702			1.911		110.2		121.8	
$^2A_1$	aD	1.711	1.719	1.912	1.834	1.996	109.3	115.4	104.1	87.1
	aT-ECP	1.702	1.710	1.906	1.827	1.990	109.3	115.3	103.5	86.2
$^2B_2$	aD	1.716	1.711	1.890	1.957	1.874	113.1	108.8	93.6	108.0
	aT-ECP	1.707	1.702	1.884	1.953	1.867	113.1	108.8	93.9	107.3
					$Mo_3O_9^{2-}$					
$^1A_1'$	aD	1.734			1.920		113.4		132.8	
	aT-ECP	1.726			1.914		113.4		132.7	
$^3A_2'$	aD	1.741			1.916		115.0		95.8	
	aT-ECP	1.733			1.908		115.1		94.8	
$^1A_1$ (***a***)	aD	1.737	1.745	1.938	1.835	1.969	112.5	117.8	104.8	79.5
	aT-ECP	1.728	1.736	1.932	1.826	1.967	112.5	117.9	104.6	79.0
$^1A_1$ (***b***)	aD	1.742	1.735	1.886	2.018	1.850	116.5	109.5	88.1	109.9
	aT-ECP	1.733	1.726	1.880	2.01 5	1.842	116.5	109.6	87.6	109.3
$^3A_1$	aD	1.736	1.741	1.929	1.894	1.981	112.6	115.2	120.9	90.4
	aT-ECP	1.727	1.732	1.922	1.887	1.976	112.7	115.2	121.2	89.6
$^3B_2$	aD	1.742	1.737	1.943	1.988	1.845	116.1	110.8	93.5	101.4
	aT-ECP	1.733	1.728	1.939	1.982	1.838	116.0	110.9	92.5	100.9
					W_3O_9					
$^1A_1'$	aD	1.706			1.905		108.2		103.5	
	aT-ECP	1.706			1.908		108.2		102.9	
					$W_3O_9^-$					
$^2A_1'$	aD	1.724			1.921		109.7		124.1	
	aT-ECP	1.724			1.923		109.7		123.8	
$^2A_1$	aD	1.726	1.729	1.914	1.837	2.014	109.5	113.1	104.0	82.7
	aT-ECP	1.727	1.730	1.916	1.838	2.017	109.5	113.2	103.5	82.2
$^2B_2$	aD	1.730	1.726	1.895	1.964	1.876	112.5	109.1	90.8	108.2
	aT-ECP	1.731	1.727	1.898	1.968	1.878	112.6	109.1	90.4	107.5
					$W_3O_9^{2-}$					
$^1A_1'$	aD	1.746			1.927		112.4		134.6	
	aT-ECP	1.747			1.928		112.5		134.2	
$^3A_2'$	aD	1.75 3			1.917		113.9		91.7	
	aT-ECP	1.75 5			1.920		114.0		91.2	
$^1A_1$ (***a***)	aD	1.749	1.753	1.939	1.833	1.995	111.9	115.3	104.8	75.3
	aT-ECP	1.750	1.753	1.941	1.835	2.001	111.9	115.3	104.6	75.0
$^1A_1$ (***b***)	aD	1.751	1.748	1.897	2.032	1.850	114.5	109.8	84.7	109.2
	aT-ECP	1.752	1.749	1.900	2.036	1.852	114.5	109.8	84.5	108.7
$^3A_1$	aD	1.748	1.748	1.938	1.896	1.992	112.4	112.7	124.6	86.2
	aT-ECP	1.749	1.749	1.939	1.897	1.995	112.5	112.8	124.4	85.8
$^3B_2$	aD	1.753	1.751	1.902	1.899	1.981	113.4	114.0	94.0	90.2
	aT-ECP	1.753	1.752	1.901	1.892	1.985	113.3	114.1	94.1	90.1

[a] Geometric parameters listed are shown in Figure 1.

by more than 14 kcal/mol for M = Mo and more than 30 kcal/mol for M = W. With core-valence correlation corrections, the other states are destabilized by 2−4 kcal/mol relative to the $^1A_1'$ state. The $^1A_1'$ state of $M_3O_9^{2-}$ was predicted to be 9.1 kcal/mol higher in energy than the $^2A_1$ state of $M_3O_9^-$ for M = Mo, but 2.4 kcal/mol lower in energy for M = W at the CCSD(T)/aT level, so that $W_3O_9^{2-}$ is a stable dianion relative to the monoanion. The inclusion of core-valence correlation corrections further stabilizes $Mo_3O_9^{2-}$ and $W_3O_9^{2-}$ by 3.2 and 3.1 kcal/mol, respectively. Thus, $Mo_3O_9^{2-}$ now has a negative electron affinity of 5.9 kcal/mol and $W_3O_9^{2-}$ has a positive electron affinity of 5.5 kcal/mol without extrapolation to the CBS limit, which is expected to further stabilize the dianion. The CCSD(T)/aD method slightly underestimates the energy differences at the CCSD(T)/aT level between the $^2A_1'$ and $^2A_1$ states by ~1 kcal/mol, whereas the B3LYP/aD method slightly overestimates them by a similar amount.

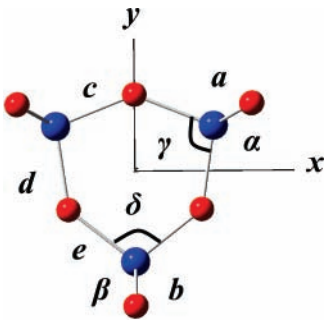

Figure 1. Schematic of the structure of $M_3O_9^{n-}$ (M = Mo, W; $n = 0-2$). In D_{3h} symmetry, the *z*-axis is the threefold axis pointing out of the plane of the page, whereas in C_{2v} symmetry, the *y*-axis is taken as the twofold axis to correlate the orbitals in these two symmetries.

Electron Detachment Energies. The calculated ADEs and VDEs at the B3LYP and CCSD(T) levels for $M_3O_9^-$ are listed in Table 3 and are compared to the experimental values.[3] Because of the large geometry changes upon electron detachment, the photoelectron spectrum for the transition from the ground state of the anion to that of the neutral cluster exhibits a very broad profile. This prevents the accurate location of the adiabatic transition and, to a lesser extent, the vertical transition.

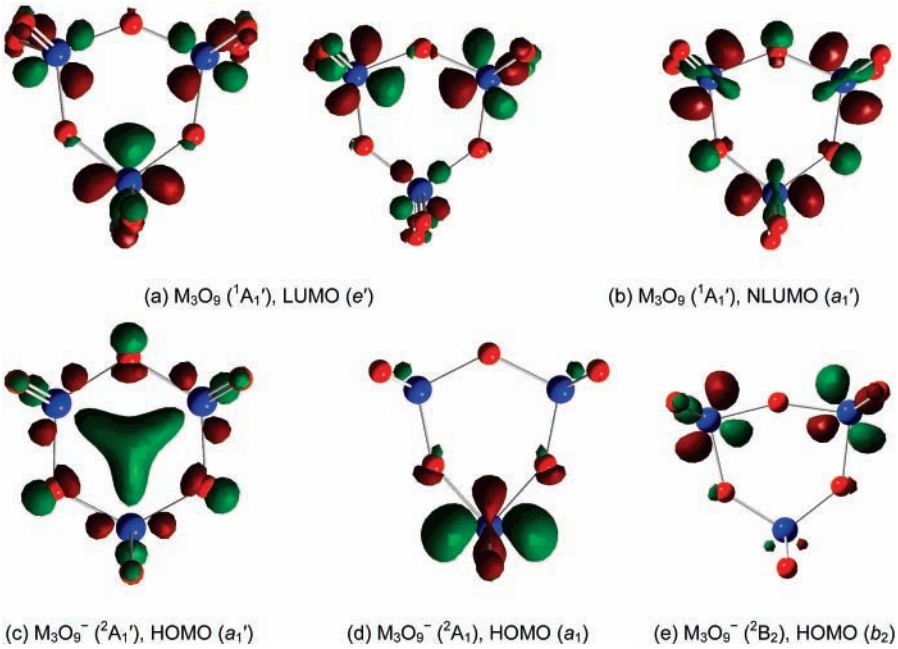

Figure 2. First three LUMOs of the $^1A_1'$ state of M_3O_9 (M = Mo, W) and the SOMOs of the $^2A_1'$, $^2A_1$, and $^2B_2$ states of $M_3O_9^-$ at the B3LYP/aD level.

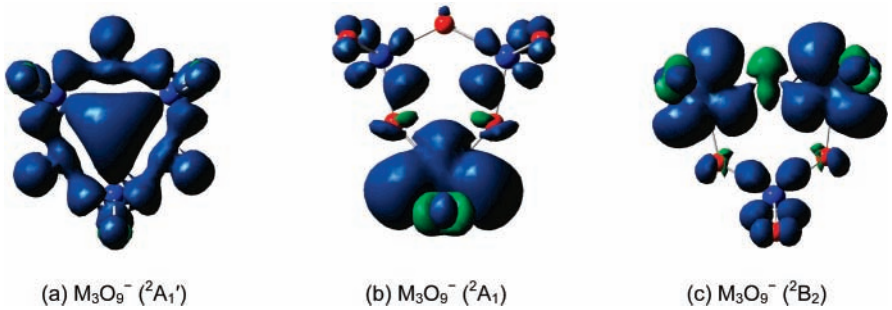

Figure 3. Total electron spin densities of the $^2A_1'$, $^2A_1$, and $^2B_2$ states of $M_3O_9^-$ at the B3LYP/aD level.

TABLE 2: Relative Energies in Kilocalories per Mole for the Electronic States of $M_3O_9^-$ (M = Mo, W) with Respect to the $^2A_1$ State and $M_3O_9^{2-}$ with Respect to the $^1A_1'$ State at the B3LYP and CCSD(T) Levels

	$M_3O_9^-$			$M_3O_9^{2-}$					
	$^2A_1$	$^2B_2$	$^2A_1'$	$^1A_1'$	$^3A_2'$	$^1A_1$ (***a***)	$^1A_1$ (***b***)	$^3A_1$	$^3B_2$
				M = Mo					
B3LYP/aD	0.0	1.4	8.2	0.0	13.1	14.2	15.4	20.5	13.9
B3LYP/aT-ECP	0.0	1.6	8.7	0.0	13.9	14.6	15.8	21.6	14.6
CCSD(T)/aD[a]	0.0	3.0	6.5	0.0	24.1	18.6	16.1	29.0	23.8
CCSD(T)/aT[a]	0.0		7.5	0.0		17.7	15.2		
CCSD(T)/aT[a] + CV[b]	0.0		6.3	0.0		20.2	19.1		
CCSD(T)/aD-ECP[c]	0.0	3.3	6.4	0.0	23.1	16.8	14.4	26.1	21.1
CCSD(T)/aT-ECP[c]	0.0		8.2	0.0		17.2	14.6		
				M = W					
B3LYP/aD	0.0	3.1	2.6	0.0	34.9	29.6	31.7	34.1	35.0
B3LYP/aT-ECP	0.0	3.2	3.3	0.0	33.5	28.6	30.7	33.2	33.8
CCSD(T)/aD[a]	0.0	5.9	0.2	0.0	50.8	37.1	34.0	42.1	47.5
CCSD(T)/aT[a]	0.0		1.1	0.0		36.1	33.0		
CCSD(T)/aT[a] + CV[b]	0.0		−0.1	0.0		38.2	36.4		
CCSD(T)/aD-ECP[c]	0.0	6.1	1.4	0.0	43.5	33.4	29.7	38.2	43.0
CCSD(T)/aT-ECP[c]	0.0		2.1	0.0		34.3	31.0		

[a] B3LYP/aD geometries. [b] CCSD(T)/aug-cc-pwCVDZ/aug-cc-pwCVDZ-PP. [c] B3LYP/aT-ECP geometries.

For M = Mo, the calculated VDE at the CCSD(T)/aT level is smaller than the experimental value by ~0.1 eV for the $^2A_1$ state and by ~0.2 eV for the $^2A_1'$ state. At the B3LYP/aD level, they are essentially identical and both are larger than the experimental value by ~0.2 eV. For M = W, the calculated VDE for the $^2A_1'$ state at the CCSD(T)/aT level is essentially identical to the experimental value, whereas that for the $^2A_1$ state is ~0.4 eV lower. The VDEs from the B3LYP/aD calculations are larger than the experimental value by ~0.2 eV for the $^2A_1'$ state but smaller by ~0.2 eV for the $^2A_1$ state. The CCSD(T)/aD results are smaller than the CCSD(T)/aT results by ~0.1 eV. In terms of the ADEs, the CCSD(T)/aT results

TABLE 3: Experimental and Calculated ADEs and VDEs in Electronvolts for $M_3O_9^-$ (M = Mo, W)

	ADE(Mo)		VDE(Mo)		ADE(W)		VDE(W)	
approach	$^2A_1$	$^2A_1'$	$^2A_1$	$^2A_1'$	$^2A_1$	$^2A_1'$	$^2A_1$	$^2A_1'$
B3LYP/aD	3.52	3.17	4.17	4.16	3.23	3.12	4.06	4.44
B3LYP/aT-ECP	3.42	3.05	4.09	4.11	3.20	3.05	4.03	4.40
CCSD(T)/aD[a]	3.32	2.95	3.80	3.69	2.99	2.98	3.73	4.09
CCSD(T)/aT[a]	3.24	2.91	3.88	3.81	2.98	2.93	3.78	4.19
CCSD(T)/aT[a] + CV[b]	3.29	3.01	3.92	3.85	3.04	3.04	3.85	4.22
CCSD(T)/aD-ECP[c]	3.33	3.05	3.72	3.56	3.05	3.00	3.71	3.94
CCSD(T)/aT-ECP[c]	3.16	2.81	3.79	3.72	2.99	2.89	3.76	4.11
experimental[d]	3.5		4.0		3.5		4.2	

[a] B3LYP/aD geometries. [b] CCSD(T)/aug-cc-pwCVDZ/aug-cc-pwCVDZ-PP. [c] B3LYP/aT-ECP geometries. [d] Reference 3.

are smaller than the experimental values by 0.25 eV for the $^2A_1$ state of $Mo_3O_9^-$ and by 0.5−0.6 eV for all of the other states. This indicates that the reported ADEs should be best considered as upper limits. The effect of core-valence correlation corrections is in general to increase the ADE and VDE to bring them into better agreement with experiment. For the $^2A_1$ ground state for $Mo_3O_9^-$, the increase in the ADE is 0.05 eV, and it is 0.04 eV in the VDE. For the $^2A_1'$ state for $Mo_3O_9^-$, the ADE increases by 0.10 eV and the VDE by a smaller amount of 0.04 eV. For the $^2A_1$ state for $W_3O_9^-$, the increase in the ADE is 0.06 eV, and it is 0.07 eV in the VDE. For the $^2A_1'$ state for $W_3O_9^-$, the ADE increases by 0.11 eV and the VDE by a smaller amount of 0.03 eV similar to that for $Mo_3O_9^-$.

We can use results from a recent benchmark study[56] on the electron affinities of the monomers and dimers of the group VIB metal oxide clusters to estimate the effects of extrapolating the CCSD(T) energies to the complete basis set (CBS). In that study, we found excellent agreement between experiment[57] and CCSD(T)/CBS values including core-valence correlation corrections for the electron affinities of MoO_3, WO_3, and W_2O_6. Compared to the CCSD(T)/aT results, the following effects were observed for the CCSD(T)/CBS values. For MoO_3, basis set extrapolation effect on the VDE is only +0.042 eV, whereas for Mo_2O_6, it is +0.068 eV. For WO_3, there is a +0.041 eV basis set extrapolation effect, and for W_2O_6, there is a +0.057 eV basis set extrapolation effect. Thus, we estimate that the VDEs of $M_3O_9^-$ will increase by ~0.1 eV when extrapolated to the CBS limit. For $Mo_3O_9^-$, this leads to good agreement with experiment within 0.1 eV (4.02 eV for the $^2A_1$ state and 3.95 eV for the $^2A_1'$ state versus 4.0 eV from experiment), which is within the experimental uncertainty for either state. We note that one cannot use the VDEs to distinguish between the two states for $Mo_3O_9^-$ because they are very close in energy with a difference of less than 0.1 eV. For $W_3O_9^-$, the difference in the VDEs for the two states was predicted to be ~0.4 eV at the CCSD(T)/aT level with core-valence correlation corrections. The correction for the basis set extrapolation brings the predicted value for the $^2A_1$ state to within 0.25 eV of experiment from below, whereas for the $^2A_1'$ state, the value is ~0.12 eV too large. Thus, both values are still close to the experimental value considering errors in the calculations and in the experiments, although the results may slightly favor the $^2A_1'$ state. The changes due to basis set extrapolation for the ADEs are expected to be smaller, on the order of +0.05 eV (the basis set extrapolation effects from the aT basis set to the CBS limit are 0.012, 0.019, 0.023, and 0.030 eV for MoO_3, Mo_2O_6, WO_3, and W_2O_6, respectively), which will slightly improve the agreement with experiment.

An estimate of the potential for significant multireference character in the wavefunction can be obtained from the T_1 diagnostic[58] from the CCSD calculation. The T_1 diagnostics are given as Supporting Information. The T_1 values for most of the molecules containing Mo as the metal with the aD basis sets are on the order of 0.03 to 0.04, suggesting minimal multireference character except for $Mo_3O_9^{2-}$ ($^1A_1$ (***a***)), which has a value of 0.051, suggesting some multireference character. The T_1 diagnostics for most of the molecules containing W as the metal with the aD basis sets are smaller, near 0.03 except for $W_3O_9^{2-}$ ($^1A_1$ (***a***)), which has a value of 0.042 and $W_3O_9^{2-}$ ($^3A_2'$) with a value of 0.051. We note that there is some dependence of T_1 on the form of the metal basis set and ECP as the values with the aD-ECP basis are somewhat smaller than the values with the aD basis.

DFT Predictions of Detachment Energies. Table 4 presents the calculated energy differences for the $^2A_1'$ and $^2A_1$ states and their ADEs and VDEs with various DFT exchange-correlation functionals at the B3LYP geometries. For M = Mo, most DFT functionals predict the $^2A_1$ state to be lower in energy except for the local functionals SVWN5 and BB95. In the most extreme case, the BMK functional predicts the $^2A_1$ state to be 21.6 kcal/mol more stable than the $^2A_1'$ state. The situation for M = W is more complicated. All of the pure DFT functionals predict the $^2A_1'$ state to be lower in energy except for BLYP. Among the hybrid DFT functionals, the B3P86, B3PW91, B1B95, B972, PBE1PBE, and O3LYP functionals predict these two states to have essentially the same energy, the B3LYP, B1LYP, mPW1PW91, B98, B971, and BMK functionals predict the $^2A_1$ state to be lower in energy, whereas the TPSSh functional predicts the $^2A_1'$ state to be lower in energy. For the calculated VDEs of the $^2A_1$ state, those from the SVWN5, B1B95, B1LYP, B98, B971, and B972 functionals are within 0.1 eV of the experimental value for M = Mo. For M = W, only the mPW1PW91 and BMK functionals give values within 0.1 eV from the experimental measurement. The predicted VDEs for the $^2A_1'$ state are slightly smaller by ~0.1 eV or essentially identical to those for the $^2A_1$ state for M = Mo except for the SVWN5 and BMK methods. For M = W, the calculated VDEs for the $^2A_1'$ state are larger than those for the $^2A_1$ state by ~0.4 eV, and they are within 0.1 eV of the experimental value for many functionals. Most of these functionals also give excellent values for the VDE of $W_2O_6^-$ within 0.1 eV from the experimental value.[56]

Implications for Cluster Reactivity. The results from the CCSD(T) and DFT calculations indicate that the $^2A_1$ and $^2A_1'$ states of $W_3O_9^-$ lie extremely close in energy and should coexist under the experimental conditions. Furthermore, the VDEs for both states are close to the experimental values, so that one cannot exclude the contribution from either state to the observed spectra. The analysis of the experimental data is further complicated because the Franck−Condon factors for overlap of the anion with the neutral molecule could be quite different

TABLE 4: Energy Difference between the $^2A_1'$ and $^2A_1$ States in Kilocalories per Mole, $\Delta E = E(^2A_1') - E(^2A_1)$, and Their ADEs and VDEs in Electronvolts for $M_3O_9^-$ Calculated with Various Density Functional Methods as Compared to the CCSD(T)/aT and Experimental Results[a]

	ΔE(Mo)	ADE(Mo)		VDE(Mo)		ΔE(W)	ADE(W)		VDE(W)	
method		$^2A_1$	$^2A_1'$	$^2A_1$	$^2A_1'$		$^2A_1$	$^2A_1'$	$^2A_1$	$^2A_1'$
B3LYP	9.3	3.43	3.02	4.16	4.15	3.6	3.17	3.02	4.03	4.44
B3P86	6.1	3.90	3.64	4.71	4.71	−0.2	3.65	3.66	4.61	5.03
B3PW91	6.0	3.32	3.06	4.11	4.12	−0.4	3.07	3.09	4.02	4.45
B1B95	7.4	3.21	2.89	4.01	4.06	0.1	2.99	2.95	3.95	4.37
B1LYP	11.1	3.38	2.90	4.07	4.04	5.4	3.07	2.83	3.94	4.35
mPW1PW91	7.3	3.40	3.08	4.18	4.16	0.3	3.09	3.07	4.08	4.51
B98	8.0	3.30	2.95	4.08	4.09	1.4	3.02	2.96	3.95	4.39
B971	7.4	3.25	2.93	3.99	4.02	0.7	2.95	2.93	3.86	4.32
B972	6.4	3.10	2.83	3.92	3.97	−0.2	2.88	2.89	3.86	4.32
PBE1PBE	6.8	3.37	3.07	4.14	4.16	−0.3	3.04	3.05	4.04	4.49
O3LYP	5.6	3.05	2.81	3.80	3.88	−0.2	2.81	2.82	3.73	4.15
TPSSh	4.4	3.26	3.07	3.89	3.97	−2.1	2.96	3.06	3.82	4.27
BMK	21.6	3.75	2.82	4.59	4.25	8.8	3.18	2.80	4.15	4.58
SVWN5	−2.7	3.22	3.33	3.94	4.15	−8.7	3.00	3.37	3.92	4.38
BLYP	4.2	3.12	2.94	3.56	3.68	0.4	2.93	2.92	3.58	3.98
BP86	1.2	3.27	3.22	3.82	3.93	−4.1	3.05	3.23	3.82	4.21
BPW91	1.3	3.14	3.08	3.71	3.80	−4.6	2.91	3.11	3.68	4.09
BB95	−0.1	3.03	3.04	3.57	3.72	−5.6	2.80	3.04	3.54	3.94
PW91	1.2	3.22	3.17	3.79	3.90	−4.8	2.99	3.20	3.77	4.19
mPWPW91	1.3	3.19	3.13	3.75	3.86	−4.6	2.95	3.16	3.73	4.14
PBE	0.8	3.13	3.10	3.70	3.82	−5.1	2.91	3.13	3.69	4.11
OLYP	3.0	2.88	2.75	3.53	3.62	−2.4	2.64	2.75	3.47	3.88
TPSS	2.0	3.16	3.07	3.74	3.83	−3.9	2.91	3.08	3.68	4.12
VSXC	4.8	3.23	3.02	3.82	3.87	−1.9	2.98	3.07	3.75	4.20
HCTH93	2.4	2.98	2.88	3.67	3.77	−2.6	2.76	2.87	3.63	4.02
HCTH147	2.6	3.19	3.08	3.86	3.96	−3.1	2.96	3.09	3.81	4.23
HCTH407	3.5	3.19	3.03	3.89	3.98	−2.0	2.97	3.05	3.84	4.27
CCSD(T)/aT + CV[b]	6.3	3.29	3.01	3.92	3.85	−0.1	3.04	3.04	3.85	4.21
experimental		3.5		4.0			3.5		4.2	

[a] Geometries optimized at the B3LYP/aD level were used. [b] CCSD(T)/aug-cc-pwCVDZ/aug-cc-pwCVDZ-PP.

for the $^2A_1'$ and $^2A_1$ states of the anion, leading to different widths and intensities.

The above calculations provide insights into the behavior of these transition-metal oxide clusters. An interesting conclusion is that when an electron is transferred into the trimer cluster to form an anion, the electron can access at least two sets of low-lying virtual orbitals. The resulting anion states have substantially different spin distributions which could have significant effects on their catalytic behavior as the localized excess spin in the $^2A_1$ state could lead to higher reactivity than the delocalized spin in the $^2A_1'$ state. The fact that the two states are so close to each other means that external perturbations could favor one state over the other, leading to different reactivity characteristics and catalytic behavior.

It is clear that the addition of one electron to the vacant metal d orbitals can lead to different occupancies, either localized or delocalized, and, for M = W, that the two states are of essentially equal energy. The addition of a second electron to the metal d orbitals to form the dianion clearly leads to the stabilization of a delocalized HOMO for the ground-state singlet of the dianion. In the simplest model of these systems, the metals are in the +6 oxidation state and the O atoms in the −2 oxidation state. Thus, the metal d orbitals are nominally empty in the neutral and are separated from the oxygen p orbitals. We can then apply an approximate $4n + 2$ electron counting rule to these systems for occupying the d orbitals. For $n = 2$, the dianion could then be considered as being aromatic as discussed previously.[3] We note that there is substantial stabilization of the singlet over the triplet for the dianion so that the spin-pairing stabilization of the delocalized orbital is important. The delocalized HOMO in the dianion is consistent with the aromaticity arguments given previously.[3] In addition, $W_3O_9^{2-}$ was predicted to be a stable dianion consistent with additional stability due to its aromatic character.

Conclusions

Our coupled cluster calculations including core-valence correlation corrections predict the Jahn−Teller distorted $^2A_1$ state to be the ground state of $Mo_3O_9^-$ and that the $^2A_1$ and $^2A_1'$ states are of essentially the same energy for $W_3O_9^-$. We found that different DFT exchange-correlation functionals yield qualitatively different results for $W_3O_9^-$, where the two electronic states were predicted to be very close in energy with the coupled cluster method. With core-valence correlation corrections and estimates for the basis set extrapolation corrections included, the CCSD(T) method gives good agreement with the experimental electron detachment energies. However, the detachment energies for both the $^2A_1$ and $^2A_1'$ states are close to the experimental values, preventing exclusion of either state from contributing to the experimental spectrum based on such a comparison. $M_3O_9^{2-}$ was predicted to be a delocalized singlet in its ground electronic state, and it was calculated to be less stable than $M_3O_9^-$ for M = Mo, but more stable for M = W. The existence of many low-lying states for these species may have significant implication on the cluster reactivity, which can contribute to the catalytic activity of these transition-metal oxide clusters.

Acknowledgment. We thank Prof. Lai-Sheng Wang (Washington State University) for valuable discussions on the topic of d orbital aromaticity and Prof. K. Peterson (Washington State University) for providing the Mo and W basis sets before publication. This work was supported by the Chemical Sciences, Geosciences and Biosciences Division, Office of Basic Energy

Sciences, U.S. Department of Energy (DOE) under Grant No. DE-FG02-03ER15481 (catalysis center program). D.A.D. also thanks the Robert Ramsay Chair Fund of The University of Alabama for support. Part of this work was performed at the W. R. Wiley Environmental Molecular Sciences Laboratory, a national scientific user facility sponsored by DOE's Office of Biological and Environmental Research and located at Pacific Northwest National Laboratory, operated for the DOE by Battelle.

Supporting Information Available: Zero-point energies and electronic energies (E_e) at different computational levels calculated with the B3LYP/aD and B3LYP/aT-ECP optimized geometries. The T_1 diagnostics in the CCSD(T) calculations are also listed. Cartesian coordinates in angstroms for the different electronic states of $M_3O_9^{n-}$ (M = Mo, W; $n = 0-2$) at the B3LYP/aD and B3LYP/aT-ECP levels. This material is available free of charge via the Internet at http://pubs.acs.org.

References and Notes

(1) (a) Schleyer, P. v. R. *Chem. Rev.* **2005**, *105*, 3433. (b) Boldyrev, A. I.; Wang, L.-S. *Chem. Rev.* **2005**, *105*, 3716.

(2) Sun, Q.; Rao, B. K.; Jena, P.; Stolcic, D.; Kim, Y. D.; Gantefor, G.; Castleman, A. W., Jr. *J. Chem. Phys.* **2004**, *121*, 9417.

(3) Huang, X.; Zhai, H.-J.; Kiran, B.; Wang, L.-S. *Angew. Chem., Int. Ed.* **2005**, *44*, 7251.

(4) Parr, R. G.; Yang, W. *Density Functional Theory of Atoms and Molecules;* Oxford University Press: New York, 1989.

(5) *Density Functional Methods in Chemistry;* Labanowski, J., Andzelm, J., Eds.; Springer-Verlag: New York, 1991.

(6) Becke, A. D. *Phys. Rev. A* **1988**, *38*, 3098.

(7) Becke, A. D. *J. Chem. Phys.* **1993**, *98*, 5648.

(8) Lee, C.; Yang, W.; Parr, R. G. *Phys. Rev. B* **1988**, *37*, 785.

(9) Schleyer, P. v. R.; Maerker, C.; Dransfeld, A.; Jiao, H.; Hommes, N. J. R. v. E. *J. Am. Chem. Soc.* **1996**, *118*, 6317.

(10) Li, S.; Dixon, D. A. *J. Phys. Chem. A* **2006**, *110*, 6231.

(11) Dunning, T. H., Jr. *J. Chem. Phys.* **1989**, *90*, 1007.

(12) Kendall, R. A.; Dunning, T. H., Jr.; Harrison, R. J. *J. Chem. Phys.* **1992**, *96*, 6796.

(13) Andrae, D.; Haeussermann, U.; Dolg, M.; Stoll, H.; Preuss, H. *Theor. Chim. Acta* **1990**, *77*, 123.

(14) (a) Jamorski, C.; Casida, M. E.; Salahub, D. R. *J. Chem. Phys.* **1996**, *104*, 5134. (b) Bauernschmitt, R.; Ahlrichs, R. *Chem. Phys. Lett.* **1996**, *256*, 454. (c) Bauernschmitt, R.; Häser, M.; Treutler, O.; Ahlrichs, R. *Chem. Phys. Lett.* **1997**, *264*, 573.

(15) Hirata, S.; Head-Gordon, M. *Chem. Phys. Lett.* **1999**, *314*, 291.

(16) (a) Casida, M. E.; Salahub, D. R. *J. Chem. Phys.* **2000**, *113*, 8918. (b) Hirata, S.; Zhan, C.-G.; Aprà, E.; Windus, T. L.; Dixon, D. A. *J. Phys. Chem. A* **2003**, *107*, 10154. (c) Zhan, C.-G.; Nicholas, J. A.; Dixon, D. A. *J. Phys. Chem. A* **2003**, *107*, 4184.

(17) Purvis, G. D., III; Bartlett, R. J. *J. Chem. Phys.* **1982**, *76*, 1910.

(18) Raghavachari, K.; Trucks, G. W.; Pople, J. A.; Head-Gordon, M. *Chem. Phys. Lett.* **1989**, *157*, 479.

(19) Watts, J. D.; Gauss, J.; Bartlett, R. J. *J. Chem. Phys.* **1993**, *98*, 8718.

(20) Bartlett, R. J.; Musial, M. *Rev. Mod. Phys.* **200**7, *79*, 291.

(21) Slater, J. C. *Quantum Theory of Molecules and Solids;* McGraw-Hill: New York, 1974; Vol. 4.

(22) Vosko, S. H.; Wilk, L.; Nusair, M. *Can. J. Phys.* **1980**, *58*, 1200.

(23) Perdew, J. P. *Phys. Rev. B* **1986**, *33*, 8822.

(24) Perdew, J. P.; Wang, Y. *Phys. Rev. B* **1991**, *45*, 13244.

(25) Becke, A. D. *J. Chem. Phys.* **1996**, *104*, 1040.

(26) Burke, K.; Perdew, J. P.; Wang. Y. In *Electronic Density Functional Theory: Recent Progress and New Directions;* Dobson, J. F., Vignale, G., Das, M. P., Eds.; Plenum: New York, 1998.

(27) Adamo, C.; Barone, V. *J. Chem. Phys.* **1998**, *108*, 664.

(28) Perdew, J. P.; Burke, K.; Ernzerhof, M. *Phys. Rev. Lett.* **1996**, *77*, 3865.

(29) Perdew, J. P.; Burke, K.; Ernzerhof, M. *Phys. Rev. Lett.* **1997**, *78*, 1396.

(30) Handy, N. C.; Cohen, A. J. *Mol. Phys.* **2001**, *99*, 403.

(31) Tao, J. M.; Perdew, J. P.; Staroverov, V. N.; Scuseria, G. E. *Phys. Rev. Lett.* **2003**, *91*, 146401.

(32) Cohen, A. J.; Handy, N. C. *Mol. Phys.* **2001**, *99*, 607.

(33) Bohmann, J. A.; Weinhold, F.; Farrar, T. C. *J. Chem. Phys.* **1997**, *107*, 1173.

(34) Ruud, K.; Helgaker, T.; Bour, P. *J. Phys. Chem. A* **2002**, *106*, 7448.

(35) Helgaker, T.; Ruud, K.; Bak, K. L.; Jørgensen, P.; Olsen, J. *Faraday Discuss.* **1994**, *99*, 165.

(36) Adamo, C.; Barone, V. *Chem. Phys. Lett.* **1997**, *274*, 242.

(37) Schmider, H. L.; Becke, A. D. *J. Chem. Phys.* **1998**, *108*, 9624.

(38) Hamprecht, F. A.; Cohen, A. J.; Tozer, D. J.; Handy, N. C. *J. Chem. Phys.* **1998**, *109*, 6264.

(39) Wilson, P. J.; Bradley, T. J.; Tozer, D. J. *J. Chem. Phys.* **2001**, *115*, 9233.

(40) Van Voorhis, T.; Scuseria, G. E. *J. Chem. Phys.* **1998**, *109*, 400.

(41) Boese, A. D.; Martin, J. M. L. *J. Chem. Phys.* **2004**, *121*, 3405.

(42) Frisch, M. J.; Trucks, G. W.; Schlegel, H. B.; Scuseria, G. E.; Robb, M. A.; Cheeseman, J. R.; Montgomery, J. A., Jr.; Vreven, T.; Kudin, K. N.; Burant, J. C.; Millam, J. M.; Iyengar, S. S.; Tomasi, J.; Barone, V.; Mennucci, B.; Cossi, M.; Scalmani, G.; Rega, N.; Petersson, G. A.; Nakatsuji, H.; Hada, M.; Ehara, M.; Toyota, K.; Fukuda, R.; Hasegawa, J.; Ishida, M.; Nakajima, T.; Honda, Y.; Kitao, O.; Nakai, H.; Klene, M.; Li, X.; Knox, J. E.; Hratchian, H. P.; Cross, J. B.; Bakken, V.; Adamo, C.; Jaramillo, J.; Gomperts, R.; Stratmann, R. E.; Yazyev, O.; Austin, A. J.; Cammi, R.; Pomelli, C.; Ochterski, J. W.; Ayala, P. Y.; Morokuma, K.; Voth, G. A.; Salvador, P.; Dannenberg, J. J.; Zakrzewski, V. G.; Dapprich, S.; Daniels, A. D.; Strain, M. C.; Farkas, O.; Malick, D. K.; Rabuck, A. D.; Raghavachari, K.; Foresman, J. B.; Ortiz, J. V.; Cui, Q.; Baboul, A. G.; Clifford, S.; Cioslowski, J.; Stefanov, B. B.; Liu, G.; Liashenko, A.; Piskorz, P.; Komaromi, I.; Martin, R. L.; Fox, D. J.; Keith, T.; Al-Laham, M. A.; Peng, C. Y.; Nanayakkara, A.; Challacombe, M.; Gill, P. M. W.; Johnson, B.; Chen, W.; Wong, M. W.; Gonzalez, C.; Pople, J. A. *Gaussian 03*, revision D.02; Gaussian, Inc.: Wallingford, CT, 2004.

(43) *MOLPRO, a package of ab initio programs,* version 2006.1; Werner, H.-J.; Knowles, P. J.; Lindh, R.; Manby, F. R.; Schütz, M.; Celani, P.; Korona, T.; Rauhut, G.; Amos, R. D.; Bernhardsson, A.; Berning, A.; Cooper, D. L.; Deegan, M. J. O.; Dobbyn, A. J.; Eckert, F.; Hampel C.; Hetzer, G.; Lloyd, A. W.; McNicholas, S. J.; Meyer W.; Mura, M. E.; Nicklass, A.; Palmieri, P.; Pitzer, R.; Schumann, U.; Stoll, H.; Stone, A. J.; Tarroni, R.; Thorsteinsson, T.; Universität Stüttgart, Stüttgart, Germany and University of Cardiff, Cardiff, Wales, U.K. http://www.molpro.net (September 2007).

(44) *NWChem, A Computational Chemistry Package for Parallel Computers,* version 5.0; Bylaska, E. J.; de Jong, W. A.; Kowalski, K.; Straatsma, T. P.; Valiev, M.; Wang, D.; Aprà, E.; Windus, T. L.; Hirata, S.; Hackler, M. T.; Zhao, Y.; Fan, P.-D.; Harrison, R. J.; Dupuis, M.; Smith, D. M. A.; Nieplocha, J.; Tipparaju, V.; Krishnan, M.; Auer, A. A.; Nooijen, M.; Brown, E.; Cisneros, G.; Fann, G. I.; Früchtl, H.; Garza, J.; Hirao, K.; Kendall, R.; Nichols, J. A.; Tsemekhman, K.; Wolinski, K.; Anchell, J.; Bernholdt, D.; Borowski, P.; Clark, T.; Clerc, D.; Dachsel, H.; Deegan, M.; Dyall, K.; Elwood, D.; Glendening, E.; Gutowski, M.; Hess, A.; Jaffe, J.; Johnson, B.; Ju, J.; Kobayashi, R.; Kutteh, R.; Lin, Z.; Littlefield, R.; Long, X.; Meng, B.; Nakajima, T.; Niu, S.; Pollack, L.; Rosing, M.; Sandrone, G.; Stave, M.; Taylor, H.; Thomas, G.; van Lenthe, J.; Wong, A.; Zhang, Z. Pacific Northwest National Laboratory: Richland, WA, 2006.

(45) Kendall, R. A.; Aprà, E.; Bernholdt, D. E.; Bylaska, E. J.; Dupuis, M.; Fann, G. I.; Harrison, R. J.; Ju, J.; Nichols, J. A.; Nieplocha, J.; Straatsma, T. P.; Windus, T. L.; Wong, A. T. *Comput. Phys. Commun.* **2000**, *128*, 260.

(46) Deegan, M. J. O.; Knowles, P. J. *Chem. Phys. Lett.* **1994**, *227*, 321.

(47) Knowles, P. J.; Hampel, C.; Werner, H.-J. *J. Chem. Phys.* **1993**, *99*, 5219.

(48) Rittby, M.; Bartlett, R. J. *J. Phys. Chem.* **1988**, *92*, 3033.

(49) (a) Peterson, K. A.; Figgen, D.; Dolg, M.; Stoll, H. *J. Chem. Phys.* **2007**, *126*, 124101. (b) Peterson, K. A. Washington State University, Pullman, WA. Unpublished basis sets for W, **2007**.

(50) Martin, J. M. L.; Sundermann, A. *J. Chem. Phys.* **2001**, *114*, 3408.

(51) Woon, D. E.; Dunning, T. H., Jr. *J. Chem. Phys.* **1995**, *103*, 4572.

(52) Peterson, K. A.; Dunning, T. H., Jr. *J. Chem. Phys.* **2002**, *117*, 10548.

(53) Wilson, E. B., Jr.; Decius, J. C.; Cross, P. C. *Molecular Vibrations;* Dover: New York, 1980.

(54) (a) Mead, C. A.; Truhlar, D. G. *J. Chem. Phys.* **1979**, *70*, 2284. (b) Truhlar, D. G.; Mead, C. A. *Phys. Rev. A* **2003**, *68*, 032501/1−2.

(55) Richtsmeier, S. C.; Eades, R. A.; Dixon, D. A.; Gole, J. L. In *Metal Bonding and Interactions in High Temperature Systems;* Gole, J. L., Stwalley, W. C., Eds.; ACS Symposium Series 179; American Chemical Society: Washington, DC, 1982; p 177.

(56) Li, S.; Dixon, D. A. *J. Phys. Chem. A* **2007**, in press.

(57) (a) Zhai, H.-J.; Kiran, B.; Cui, L.-F.; Li, X.; Dixon, D. A.; Wang, L.-S. *J. Am. Chem. Soc.* **2004**, *126*, 16134. (b) Zhai, H.-J.; Huang, X.; Cui, L.-F.; Li, X.; Li, J.; Wang, L.-S. *J. Phys. Chem. A* **2005**, *109*, 6019.

(58) Lee, T. J.; Taylor, P. R. *Int. J. Quantum Chem. Symp.* **1989**, *23*, 199.